



Cite this: *J. Mater. Chem. C*, 2021,
9, 2392

Construction of polysiloxane-based fluorescent probe for visualizing pH down-regulation†

Xiaoni Wang, Minggang Tian,^{ib} Zhiming Gou^{ib} and Yujing Zuo^{ib} *

Changes in the intracellular pH values constitute a significant physiological and pathological process and play vital roles in autophagy, self-repairing, and programmed cell apoptosis. A unique fluorescent probe (**PN-1**) based on polysiloxanes designed using the intramolecular charge transfer (ICT) mechanism has been developed for the detection of the pH down-regulation process for the first time. **PN-1** has been successfully applied to HeLa cells and HepG2 cells for visualizing the pH value changes in a ratiometric manner. The result presented that, in the normal intracellular autophagy process, **PN-1** displayed strong blue fluorescence while starvation induced apparent red fluorescence of **PN-1**. In addition, the inhibitory effect of chloroquine (CQ) to pH value changes during the cell starvation treatment process has been analyzed. The work indicated that a polysiloxane-based fluorescent probe could be applied to detect pH value changes during autophagy, and paved a new avenue for the further design of fluorescent probes for monitoring pH changes.

Received 17th November 2020,
Accepted 6th January 2021

DOI: 10.1039/d0tc05398h

rsc.li/materials-c

Introduction

Changes in intracellular pH values constitute a significant physiological and pathological process and play vital roles in autophagy, self-repairing, and programmed cell apoptosis.^{1–4} In a normal physiological process, the intracellular pH value is maintained within a very narrow range (7.2–7.4), while the pH value, during the starvation period, tends to decrease.^{5–8} Meanwhile, during the starvation period, pH values rapidly reach abnormal levels to counterbalance nutrient shortage through controlled self-digestion.^{9–13} Remarkably, some research studies have displayed that aberrant pH value level may be tightly linked to serious diseases such as Alzheimer's disease, Parkinson's disease and Huntington's disease.^{14–16} Therefore, it is significant to accurately monitor pH value changes in living systems.

Recently, studies have illustrated that pH value changes may be closely related to the autophagy process.^{17–20} Acidic conditions can induce and promote the autophagy process, while the increase of pH can inhibit the autophagy process by reducing the activity of hydrolase.^{21,22} Hence, it is an ingenious approach for monitoring the autophagy process by detecting the pH value changes.

Compared with the existing detection methods, fluorescence imaging technology exhibits many advantages such

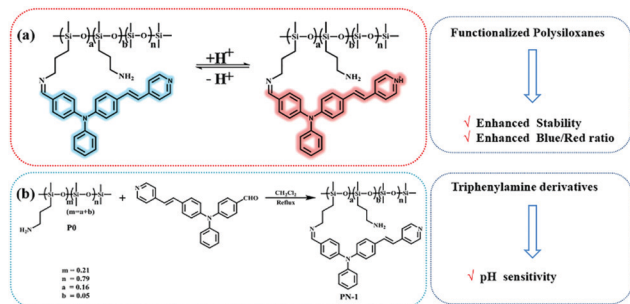
as high sensitivity, non-invasive detection and *in situ* detection. Currently, many fluorescent probes based on small organic molecules have widely received extensive attention for monitoring autophagy.^{23–26} Dong's group reported a fluorescent probe for the visual detection of lysosomal pH changes during autophagy.²¹ Tan and co-workers have constructed a ratiometric fluorescent probe for monitoring mitophagy by detecting pH changes.²⁷ However, most of the previous works are based on small molecule organic fluorescent probes, which may have undesired performance in photostability. Therefore, we are keen to design an excellent probe with superior photostability and biocompatibility. Fortunately, a macromolecular based probe is an outstanding platform for us, and we aim to investigate the role played by the polymer in pH value changes.

Polysiloxanes (PDMSs), as a unique functional polymer, have long been known to possess excellent properties including high flexibility and radiation resistance, low bio-toxicity and excellent biocompatibility.^{28,29} Moreover, PDMSs have attracted enormous interest in various fields due to the various reaction sites which are prone to be step-wise functionalized.³⁰ In addition, polysiloxanes can serve as an excellent platform to improve photostability and enhance the blue/red fluorescence ratio in the cytoplasm. Therefore, in this work, we anticipated to investigate pH down-regulation during autophagy by using a polysiloxane platform to achieve superior properties.

A novel fluorescent probe (**PN-1**) based on polysiloxanes was presented for the ratiometric monitoring of pH changes. Triphenylamine derivatives were selected as the fluorophore due to their excellent photostability and high fluorescence quantum yields.^{31,32} The pyridine moiety, in an acidic environment,

School of Chemistry and Chemical Engineering, School of Materials Science and Engineering, University of Jinan, Shandong 250022, P. R. China.
E-mail: zuoyujing0888@163.com

† Electronic supplementary information (ESI) available. See DOI: 10.1039/d0tc05398h



Scheme 1 (a) The design and pH sensing mechanism of **PN-1**; and (b) the synthetic route of **PN-1** ($m = 0.21$, $n = 0.79$, $a = 0.16$, $b = 0.05$).

will combine with hydrogen protons (H^+), which would lead to greater charge separation and lower excited state energy. Hence, the fluorescence maximum emission peak of the probe can display a red shift to achieve the purpose of controlling the fluorescence properties.³³ In addition, selecting PDMS as the foundation base of a fluorescent probe could increase the local concentration and magnify the fluorescence signal, which improves the photostability of the fluorescence signal in the complex detection environment (Scheme 1(a)).³⁴ As expected, **PN-1** demonstrated high sensitivity to pH under weak acidic conditions, excellent photostability and low cytotoxicity. Our work clarified that polysiloxane-based fluorescent probes are feasible for visualizing pH changes in the fluorescence imaging field.

Results and discussion

Experimental section

Materials. All chemicals and solvents were of analytical grade and were used without further purification. (aminopropyl)-methylmethoxysilane, dimethyldimethoxysilane, and 4-(diphenylamino)benzaldehyde were purchased from Shanghai San Chemical. 4-Vinylpyridine and *N*-bromosuccinimide were purchased from Sinopharm Chemical Reagent Co., Ltd (Shanghai, China). The HeLa cells and HepG2 cells were purchased from Procell Life Science & Technology Co. Ltd. The other reagents used in this work were purchased from the supplier, and the water used in the experiment was ultrapure water.

Absorption and fluorescence measurements. All experiments were performed in different PBS buffer solutions and Britton–Robinson (BR) buffer solutions. The stock solution of probe **PN-1** (10 μ M) was prepared in DMSO and 100 mmol solutions of different ions ($FeSO_4$, $FeCl_3$, $ZnSO_4$, $AlCl_3$, $CaCl_2$, $BaCl_2$, $MgCl_2$, $NaCl$, KCl , NH_4Cl , Na_3PO_4 , Na_2HPO_4 , Na_2SO_4 , H_2O_2 , and CQ) were prepared in aqueous solution. The fluorescence spectra were obtained by excitation at 405 nm and 460 nm. The excitation and emission slit widths were 10 nm and 10 nm, respectively.

Synthesis of PN-1. The synthetic route and the structure are shown in Scheme 1(b). **P0** (2.0 g) and **N-1** (0.378 g) were mixed in CH_2Cl_2 (20 mL). The reaction mixture was refluxed at 45 $^\circ$ C for 8 h. After being cooled to room temperature, the solvent was evaporated and **PN-1** was obtained as a light yellow viscous

liquid. Yield: 71%. 1H NMR (400 MHz, $CDCl_3$) δ 8.59–8.57 (m, 3H), 7.70 (dd, $J = 28.6$, 5.9 Hz, 2H), 7.48 (d, $J = 8.4$ Hz, 4H), 7.37 (d, $J = 4.7$ Hz, 4H), 7.14 (s, 4H), 6.96 (d, $J = 16.2$ Hz, 2H), 2.68 (t, $J = 6.9$ Hz, 30H), 1.50 (d, $J = 16.3$ Hz, 30H), 0.53 (d, $J = 8.4$ Hz, 30H), 0.09 (s, 48H). ^{13}C NMR (101 MHz, $CDCl_3$) δ 160.95, 158.61, 154.36, 152.94, 150.15, 147.95, 144.75, 141.39, 137.65, 135.77, 133.52, 132.35, 130.86, 128.82, 128.13, 124.51, 123.73, 120.67, 65.54, 19.17, 14.46, 1.00.

Results and discussion. Intramolecular charge transfer (ICT) is a common mechanism for designing fluorescent probes. The molecule usually consists of a strong electron donor–acceptor and a π -conjugation system. Herein a novel type of polysiloxane fluorescent probe was constructed for monitoring the autophagy process (Scheme 1(a)). Triphenylamine derivatives were selected to serve as the electron donor due to their excellent optical properties, and the pyridine moiety acted as the response sites for pH as the electron acceptor to compose the ICT system. Polysiloxanes were selected as the platform due to their high flexibility and radiation resistance, low biotoxicity and excellent biocompatibility. In addition, polysiloxane-based compounds showed fine stability, which is conducive to maintaining outstanding fluorescence stability of the probe in a complex detection environment. Moreover, the polysiloxane chain has eminent flexibility and could assist **PN-1** to enhance the ability to capture H^+ . Therefore, triphenylamine derivatives are bonded to polysiloxanes *via* the Schiff base structure (Scheme 1(b)).

The probe **PN-1** was characterized using standard 1H NMR (Fig. S3, ESI †), ^{13}C NMR (Fig. S4, ESI †), the infrared spectrum (Fig. S7, ESI †) and gel permeation chromatography (GPC) (Table S1 and Fig. S6, ESI †). From the standard 1H NMR analysis of **PN-1**, we observed that the characteristic peak of **N-1** (Fig. S1, ESI †) at 9.84 ppm ($-CHO$) disappeared; meanwhile, a new characteristic peak of the $-Si-CH_3$ group appeared at 0.09 ppm, indicating that **N-1** was bonded to the polysiloxane chain successfully. The molecular weight (M_n) of **PN-1** was about 5200 $g\ mol^{-1}$ tested by GPC (Table S1, ESI †), which was higher than that of **P0** (3500 $g\ mol^{-1}$). The enhancement in the molecular weight of **PN-1** indicated the success of the functionalized polysiloxanes. In the infrared spectrum (IR), compared with the spectrum of polysiloxanes, the characteristic peak of the benzene ring appears in the spectrum at 1400–1600 cm^{-1} , also indicating that **PN-1** has been synthesized. In addition, the IR spectrum did not display significant changes in the polysiloxanes' main chain peak, revealing that the polymer skeletal structure was not involved in the reaction process. The mass spectrum (MS) of **N-1** was also obtained with a peak at 377.1643 as shown in Fig. S5 (ESI †). The result indicates that the compound **N-1** has been successfully synthesized.

Optical properties of PN-1. With the probe in hand, the optical properties of **PN-1** were explored by UV-Vis absorption in PBS buffer with different pH values (Fig. S8(a), ESI †). When the pH changed from 3.0 to 8.0, the UV absorption peak of **PN-1** at 440 nm slowly moved to 405 nm. This absorption peak shift could be attributed to the protonation of the pyridine moiety of the nitrogen atom. As shown in Fig. S8(c) (ESI †), we further tested the UV absorption properties of the probes **PN-1** and **N-1**

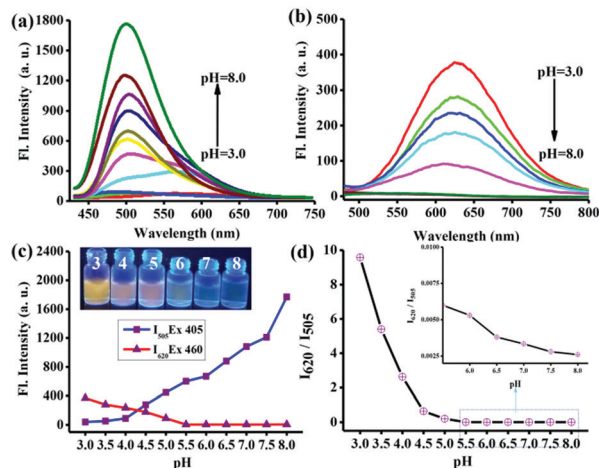


Fig. 1 The fluorescence spectra of the probe **PN-1** (10 μM) at different pH values with excitation at 405 nm (a) and 460 nm (b); (c) the dependent fluorescence intensity at 505 nm (excited by 405 nm) and 620 nm (excited by 460 nm) and the photographs of **PN-1** (pH range of 3.0–8.0) under UV lamp (365 nm); (d) the pH dependent intensity ratio at 620 nm to 505 nm. Inset: Amplification at pH values of 5.5–8.0.

in ethanol solution. The absorption peak of the probe **PN-1** and compound **N-1** at 405 nm displayed a high overlap, but in the non-conjugation region of 250–300 nm, **PN-1** showed a larger absorption difference than compound **N-1**. This phenomenon could be attributed to the special structure of the Si–O chain in **PN-1**. In the pH = 3 buffer solution, we found that **PN-1** absorption peak shifted from 405 nm to 440 nm, indicating that the introduction of the **N-1** compound into the main chain of the polysiloxanes has endowed polysiloxanes with the ability to detect pH.

As depicted in Fig. 1(a), under the excitation of 405 nm, the fluorescent intensity of **PN-1** at 505 nm gradually decreased with the pH values changed from 8.0 to 5.5. In the acidic range (5.5–3.0), the fluorescence peak intensity at 505 nm decreases under 405 nm excitation; meanwhile, the red shift of the emission was observed. As shown in Fig. 1(b), when **PN-1** was excited at 460 nm, the fluorescence intensity at 620 nm remained almost unchanged when the pH value changed from 8.0 to 5.5. The fluorescence intensity increased rapidly at 620 nm when the pH value changed from 5.5 to 3.0. As depicted in Fig. 1(c), the change curve of the fluorescence intensity of **PN-1** under different excitation wavelengths could reveal the above phenomenon more intuitively. The above phenomenon indicates that **PN-1** could respond to pH changes. As shown in Fig. 1(d), in the fluorescence intensity ratio (I_{620}/I_{505}) change curve, it can be observed that the values of the ratio decreased significantly from 9.57 to 0.006 when the pH range increased from 3.0 to 5.5. However, the values of the ratio changed slightly when the pH ranged from 5.5 to 8.0. The pK_a value was calculated to be 3.9. The results indicate that **PN-1** tended to emit blue emission in a neutral environment. However, when **PN-1** was in acidic solutions (5.0–3.0), the protonation of the pyridine moiety of the nitrogen atom occurred, displaying red fluorescence (Scheme 1(a)). The results indicated that **PN-1** could detect pH in PBS buffer solutions.

Furthermore, we tested the response of compound **N-1** to the pH experiment in Britton–Robinson (BR) buffer. As shown in Fig. S11 (ESI[†]), when excited at 405 nm, the fluorescence signals of **N-1** at 505 nm displayed a lightly decreased tendency than that of **PN-1** (Fig. S11(a), ESI[†]). Meanwhile, when excited with 460 nm, the fluorescence signals of **N-1** at 620 nm displayed a similar tendency (Fig. S11(b), ESI[†]). The results indicated that **N-1** can respond to pH changes. However, as shown in Fig. S11(f) (ESI[†]), the fluorescence intensity ratio (I_{620}/I_{505}) of **PN-1** is higher than that of **N-1**, indicating that the polysiloxane main chain in **PN-1** endowed external improvement of the ratio of red/blue fluorescence intensity.

In addition, we tested the photostability of **PN-1** and **N-1** in ethanol/PBS (v/v = 2 : 8) solution. As shown in Fig. S12 (ESI[†]), when excited at 405 nm, the fluorescence intensity of **PN-1** at 505 nm exhibited negligible variation after continuously excitation for 60 min (Fig. S12(a), ESI[†]). Compared to the **PN-1** probe, the fluorescence intensity of **N-1** obviously declined under the same conditions (Fig. S12(b), ESI[†]). The result revealed that **PN-1** has excellent photostability in solution.

Outstanding selectivity is a critical standard to estimate the application of fluorescent probes. We further investigated the effects of different biologically relevant species on the probe at different pH values. Considering that the pH in the normal physiological environment in cells is about 7.2–7.4, and during autophagy the intracellular pH changes to acidic conditions, we chose the two test systems at pH values of 4.0 and 7.4. Some common ions FeSO_4 , FeCl_3 , ZnSO_4 , AlCl_3 , CaCl_2 , BaCl_2 , MgCl_2 , NaCl , KCl , NH_4Cl , Na_3PO_4 , Na_2HPO_4 , Na_2SO_4 , H_2O_2 and CQ were added to the probe solutions. As shown in Fig. S13 (ESI[†]), obviously, various species did not cause a significant change in the fluorescence intensity of **PN-1** in the two test systems. This result indicated that **PN-1** has good specificity for pH.

Fluorescence imaging of **PN-1 in living cells.** Cytotoxicity is a crucial criterion for evaluating the application of probe for cell imaging. Therefore, we tested the cytotoxicity of **PN-1** and **N-1** using the MTT analysis method (Fig. S14, ESI[†]). The survival rate of the HeLa cells was maintained at 85% with the concentration of 30 μM . The result showed that the probes **PN-1** and **N-1** could be used in cells. Meanwhile, the cell viability of **PN-1** was higher than that of **N-1** at the same concentration level, and the reduction in toxicity could be attributed to the polysiloxanes in **PN-1**.

Photostability is one of the most significant parameters to estimate the application of fluorescent probes. Herein, we furthermore evaluated whether the polysiloxane probe **PN-1** had a greater stability compared with the small molecule fluorescent probe **N-1** in living cells. HepG2 cells were treated with **PN-1** and **N-1** for 30 min. As shown in Fig. 2, with continuous irradiation for 15 min, the fluorescence intensity of **PN-1** was still detected with no marked change in the blue and red channel. Significantly, the fluorescence signal values of **N-1** displayed a gradually declined tendency under the same conditions (Fig. S15, ESI[†]). This result proved that **PN-1** possess excellent photostability and potential for long-term imaging in living systems.

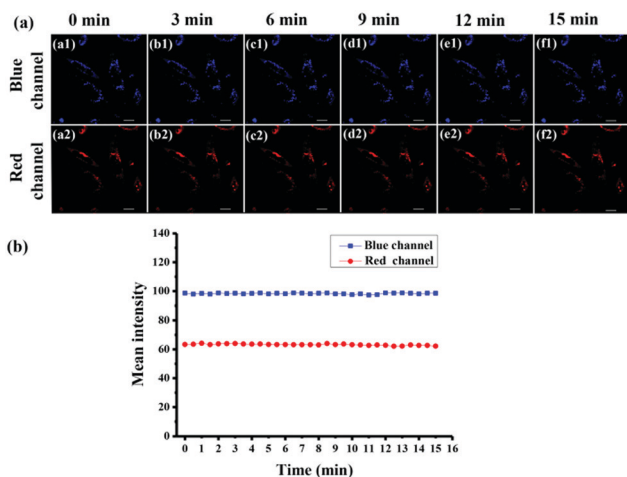


Fig. 2 (a) Fluorescence images of HepG2 cells incubated with **PN-1** ($10 \mu\text{M}$) acquired under successive excitation with a 405 nm laser and 561 nm laser (a1–f2) at different times; (b) analysis of the quantitative fluorescence intensity in (a) using Image software. The error bars represent the standard deviation ($\pm\text{S.D.}$), $n = 3$. Scale bar = $10 \mu\text{m}$.

Alterations in the extracellular pH environment will lead to changes in the intracellular pH values. Therefore, to further verify the possibility of **PN-1** response to pH in living cells (Fig. 3), HeLa cells were cultured with pH values of 4.0, 5.0, 6.0, 7.0 and 8.0, respectively. As expected, fluorescence signs in the blue channel gradually increased. Meanwhile, fluorescence sign values in the red channel gradually reduced. This phenomenon exhibited that **PN-1** can respond to pH in living cells. As depicted in Fig. S16 (ESI[†]), the pH detection in HepG2 cells was also performed with **PN-1** to test the universality and similar results were obtained. The above experimental results manifested that **PN-1** can be applied to monitor pH changes in living cells. In addition, we also obtained the ratio graph when the pH changed from 4.0 to 8.0. Converted pseudo colors were observed from red to blue in the ratiometric image, revealing that the ratio values increased. This phenomenon displayed that **PN-1** can detect intracellular pH changes in a ratiometric manner. Furthermore, we evaluated the pH sensitivity of **N-1** in

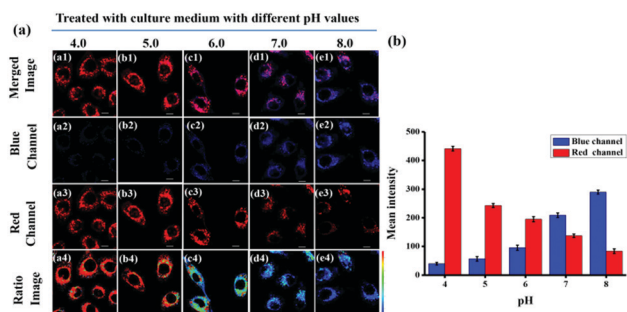


Fig. 3 (a) Fluorescence and ratiometric images of HeLa cells incubated with **PN-1** ($10 \mu\text{M}$) acquired under successive excitations using a 405 nm laser and a 561 nm laser with different pH values (a1–e4); (b) analysis of the quantitative fluorescence intensity in (a) using Image software. The error bars represent the standard deviation ($\pm\text{S.D.}$), $n = 3$. Scale bar = $10 \mu\text{m}$.

living cells. As shown in Fig. S17 (ESI[†]), at pH values from 4.0 to 8.0, the blue fluorescence intensity showed increasing tendency. The red fluorescence intensity gradually decreased in the pH range of 4.0 to 8.0. This result showed that **N-1** could respond to pH change in living cells. However, the fluorescence intensity ratio of **PN-1** was higher than that of **N-1**, revealing that polysiloxanes in **PN-1** provided external improvement to the ratio of the two channels.

We conducted the organelle targeting property test of **PN-1** in HepG2 cells. HepG2 cells were pre-incubated with $10 \mu\text{M}$ **PN-1** for 25 min, after this HepG2 cells were treated with $1 \mu\text{M}$ MitoTracker deep Red, $1 \mu\text{M}$ LysoTracker deep Red and $1 \mu\text{M}$ ER-Tracker Red for 5 min, respectively. As shown in Fig. S18 (ESI[†]), the blue signals could be attributed to **PN-1**, while the red signals were attributed to the MitoTracker deep red, the LysoTracker deep red, and the ER-tracker, respectively. Obviously, the blue fluorescence signals [Fig. S18(a2, b2, c2), ESI[†]] of **PN-1** and the red fluorescence of MitoTracker deep Red (Fig. S18(a3), ESI[†]), LysoTracker deep Red (Fig. S18(b3), ESI[†]) and ER-tracker Red (Fig. S18(c3), ESI[†]) did not show obvious overlapping. Pearson's colocalization coefficient values (R_s) of **PN-1** with MitoTracker, LysoTracker and ER-tracker were calculated to be 0.59, 0.54 and 0.62, respectively. Therefore, the staining range of **PN-1** was mainly distributed in the cytoplasm and did not exhibit a strong localization ability in main cell organelles.

Subsequently, we further evaluated the pH changes using the probe in living cells. As depicted in Fig. 4(a), the results showed that nutrient starvation conditions can aggravate the autophagy process. HeLa cells were treated with the probe in PBS buffer for 2 h and 4 h, respectively. In the control group, HeLa cells were incubated in a nutrient-containing medium for 4 h. **PN-1** displayed a strong blue fluorescence under 405 nm and a weak red fluorescence under 561 nm. There was no significant change of the intracellular pH due to the autophagy process in the nutrient medium. After starvation treatment of HeLa cells for 2 h, the blue fluorescence clearly decreased under excitation at 405 nm, and the red fluorescence enhanced dramatically when excited at 561 nm. With reference to the ratio diagram shown in Fig. 4(a), we can conclude that the pH

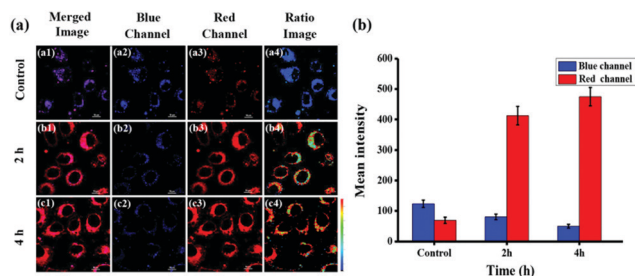


Fig. 4 The fluorescent images of HeLa cells pre-stained with **PN-1** ($10 \mu\text{M}$). (a) Then, incubated with culture medium for 2 h (control) and PBS buffer for 2 h and 4 h; (b) the mean intensity in the blue channel and red channel and the intensity ratio of the red to blue channel of the three groups of cells, bar = $10 \mu\text{m}$. The standard deviation ($\pm\text{S.D.}$), $n = 3$. Scale bar = $10 \mu\text{m}$.

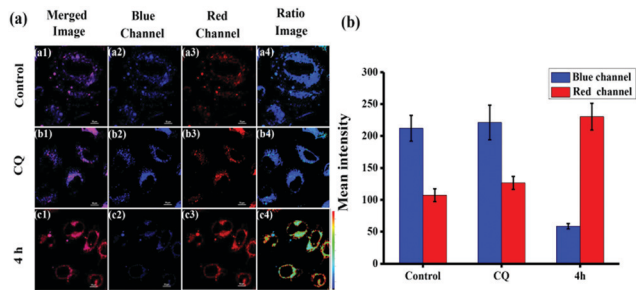


Fig. 5 The fluorescence images of HeLa cells pre-stained with **PN-1** (10 μM) for 4 h. (a) Then incubated with culture medium for 4 h (control), then incubated in PBS containing CQ (50 μM) for 4 h, and then incubated in PBS for 4 h; (b) the mean intensity in the blue channel, red channel and the intensity ratio of red to blue channel of the three groups of cells, bar = 10 μm . The standard deviation (\pm S.D.), $n = 3$. Scale bar = 10 μm .

range is about 5.0–6.0 in these cells. The imaging of HeLa cells that underwent 4 h of starvation treatment was also performed. As expected, compared to the 2 h starvation group, the blue fluorescence intensity further reduced and the red fluorescence intensity showed enhancement, which implied that the pH value further reduced to 4.0–5.0 during this period. The above phenomena indicated that compared with the cultured HeLa cells in a nutrient-containing medium, incubation of HeLa cells in PBS buffer solution without nutrients could induce the autophagy, which further led to the change of intracellular pH value. The bar graph shown in Fig. 4(b) clearly illustrates the changes in the fluorescence values of each channels that are caused by a change in the pH. Hence, in the ratiometric photograph, the blue transforms into red pseudo colors. This result showed that pH values of the HeLa cells after starvation treatment did change. We further conducted the experiment in HepG2 cells and obtained consistent results with that of HeLa cells, indicating that the pH value changes after starvation treatment were universal in living cells (Fig. S19, ESI \dagger).

CQ has been reported to possess the ability to inhibit autophagy in the starvation treatment stage in living cells.³⁵ The experiment of CQ influence ability was performed in the autophagy process. As shown in Fig. 5(a), in the control group, HeLa cells were incubated in a nutrient-containing medium for 4 h, and in the other two groups, HeLa cells were incubated in PBS buffer solution. In the CQ group, HeLa cells were treated with **PN-1** and CQ in PBS buffer solution for 4 h. In the 4 h group, HeLa cells were treated with **PN-1** in PBS buffer solution for 4 h. We clearly observed that in the control group, pH has not changed due to the presence of nutrients in the medium which inhibited the autophagy process [Fig. 5(a1–a4)]. The pH range was about 7.0–7.5 within the cells. Therefore, a strong fluorescence was displayed in the blue channel and a relative weak red fluorescence was observed in the red channel. In the experimental group (CQ group), as the existence of CQ inhibited the autophagy process, no significant change of the emission in the blue and the red channel, respectively, was observed. Even in the HeLa cells that were starvation treated in PBS buffer solution for 4 h, the blue emission was still maintained compared with that of the control group [Fig. 5(b1–b4)]. The pH

range is about 6.5–7.0 in these cells. In another experimental group, HeLa cells cultured with **PN-1** were starvation treated in PBS buffer solution for 4 h; compared with the control group, the blue fluorescence intensity in the blue channel was prominently reduced while the red fluorescence in the red channel was significantly enhanced [Fig. 5(c1–c4)]. The red pseudo color increased in the ratiometric image [Fig. 5(c4)]. The pH range was about 5.5–6.0 in these cells. Fig. 5(b) clearly shows the fluorescence intensity changes in HeLa cells. As shown in Fig. S20 (ESI \dagger), we further conducted the experiment in HepG2 cells and obtained the results similar to that in HeLa cells. The experimental results indicated that CQ possesses the ability to inhibit the autophagy progress in living cells, which also proved that the increase of pH in cells can inhibit autophagy.

Conclusion

In conclusion, a novel polysiloxane based fluorescent probe **PN-1** has been rationally constructed for the ratiometric visualization of the pH value changes. In addition, the CQ inhibitory effect on the autophagy process has also been verified. **PN-1** possessed fine properties such as low biotoxicity, excellent photostability and great biocompatibility. This work presents for the first time that a polysiloxane-based fluorescent probe can be applied to monitor pH value changes. We expect that **PN-1** can serve as an effective tool to further investigate the relationship between pH and the starvation treatment process. Meanwhile, we would like to further explore the applications of polysiloxane fluorescent probes in materials chemistry or bioscience fields.

Conflicts of interest

The authors declare no competing financial interest.

Acknowledgements

This work was financially supported by the Natural Science Foundation of China (22007037), the Natural Science Foundation of Shandong Province (ZR2018BB022, ZR2018BB058), the Foundation of Key Laboratory of Special Functional Aggregated Materials and the startup fund of the University of Jinan (1009428).

References

- 1 A. K. Thost, P. Dönnies, O. Kohlbacher and C. T. Proikas, *Methods*, 2015, **75**, 69–78.
- 2 T. L. M. Thurston, M. P. Wandel, N. Von Muhlinen, Á. Foeglein and F. Randow, *Nature*, 2012, **482**, 414.
- 3 A. M. Cuervo, E. Bergamini, U. T. Brunk, W. Dröge, M. French and A. Terman, *Autophagy*, 2005, **1**, 131–140.
- 4 X. Li, X. Liang, J. Yin and W. Lin, *Chem. Soc. Rev.*, 2021, **50**, 102–119.

- 5 B. Tang, F. Yu, P. Li, L. Tong, X. Duan, T. Xie and X. Wang, *J. Am. Chem. Soc.*, 2009, **131**, 3016–3023.
- 6 J. D. Rabinowitz and W. Eileen, *Science*, 2010, **330**, 1344–1348.
- 7 N. Mizushima, *Genes Dev.*, 2007, **21**, 2861–2873.
- 8 X. Li, X. Li and H. Ma, *Chem. Sci.*, 2020, **11**, 1617–1622.
- 9 T. Shusaku and T. Shibutani, *Cell Res.*, 2014, **24**, 58–68.
- 10 O. Yoshinori, *Cell Res.*, 2014, **24**, 9–23.
- 11 P. Jiang and N. Mizushima, *Cell Res.*, 2014, **24**, 69–79.
- 12 E. L. Eskelinen and P. Saftig, *Biochim. Biophys. Acta, Mol. Cell Res.*, 2009, **1793**, 664–673.
- 13 M. Li, A. Lee, K. L. Kim, J. Murray, A. Shrinidhi, G. Sung, K. Min and K. Kim, *Angew. Chem., Int. Ed.*, 2018, **57**, 2120–2125.
- 14 M. Qian, X. Fang and X. Wang, *Clin. Trans. Med.*, 2017, **6**, 24.
- 15 A. Tessitore and M. Pirozzi, *Pathogenetics*, 2009, **2**, 4.
- 16 H. Iwashita, S. Torii, N. Nagahora, M. Ishiyama, K. Shioji, K. Sasamoto, S. Shimazu and K. Okuma, *ACS Chem. Biol.*, 2017, **12**, 2546–2551.
- 17 D. M. Wolfe, J. H. Lee, A. Kumar, S. Lee and R. A. Nixon, *Eur. J. Neuroence.*, 2013, **37**, 1949–1961.
- 18 M. Tian, C. Liu, B. Dong, Y. Zuo and W. Lin, *Chem. Commun.*, 2019, **55**, 10440–10443.
- 19 X. Liu, Y. Su, H. Tian, L. Yang, H. Zhang and X. Song, *Anal. Chem.*, 2017, **89**, 7038–7045.
- 20 W. Wang, P. Ning, Q. Wang, W. Zhang, J. Jiang, Y. Feng and X. Meng, *J. Mater. Chem. B*, 2018, **6**, 1764–1770.
- 21 X. Wang, L. Fan, Y. Wang, C. Zhang, W. Liang, S. Shuang and C. Dong, *J. Mater. Chem. B*, 2020, **8**, 1466–1471.
- 22 P. Ning, L. Hou, Y. Feng, G. Xu, Y. Bai, H. Yu and X. Meng, *Chem. Commun.*, 2019, **55**, 1782–1785.
- 23 J. Yin, Y. Hu and J. Yoon, *Chem. Soc. Rev.*, 2015, **44**, 4619–4644.
- 24 X. Zhao, X. Chen, S. Shen, D. Li, S. Zhou, Z. Zhou, Y. Xiao, G. Xi, J. Miao and B. Zhao, *RSC Adv.*, 2014, **4**, 50318–50324.
- 25 X. Liu, Y. Su, H. Tian, L. Yang, H. Zhang, X. Song and J. W. Foley, *Anal. Chem.*, 2017, **89**, 7038–7045.
- 26 L. Xu, X. Yan and C. Yuan, *RSC Adv.*, 2018, **8**, 35289–35293.
- 27 Y. Liu, J. Zhou, L. Wang, X. Hu, X. Liu, M. Liu, Z. Cao, D. Shang and W. Tan, *J. Am. Chem. Soc.*, 2016, **138**, 12368–12374.
- 28 A. S. Fawcett, T. C. Hughes, L. Zepeda-Velazquez and M. A. Brook, *Macromolecules*, 2015, **48**, 6499–6507.
- 29 J. Chojnowski and M. Cypryk, *Silicon-Containing Polymers*, Springer, 2000, pp. 3–41.
- 30 R. I. Dmitriev and S. M. Borisov, *ACS Nano*, 2015, **9**, 5275–5288.
- 31 Y. Yan, N. Sun, F. Li, X. Jia, C. Wang and D. Chao, *ACS Appl. Mater. Interfaces*, 2017, **9**, 6497–6503.
- 32 P. S. Hariharan, E. M. Mothi, D. Moon and S. P. Anthony, *ACS Appl. Mater. Interfaces*, 2016, **8**(48), 33034–33042.
- 33 J. Herbich, M. Kijak, A. R. Zielińska, P. Thummel and J. Waluk, *J. Phys. Chem. A*, 2002, **106**, 2158–2163.
- 34 Y. Zuo, X. Wang, Z. Gou and W. Lin, *Chem. Commun.*, 2020, **56**, 1121–1124.
- 35 Y. Ma, H. Chen, B. Hao, J. Zhou, G. He, Z. Miao, Y. Xu, L. Gao, W. Zhou and Z. Zha, *J. Mater. Chem. B*, 2018, **6**, 5854–5859.